Cavity ringdown laser absorption spectroscopy and time-of-flight mass spectroscopy of jet-cooled copper silicides

J. J. Scherer, J. B. Paul, C. P. Collier, and R. J. Saykally
Department of Chemistry, University of California, Berkeley, Berkeley, California 94720

(Received 31 October 1994; accepted 20 December 1994)

The cavity ringdown technique has been implemented for electronic spectroscopy of jet-cooled CuSi produced in a pulsed UV laser vaporization plasma reactor. A time-of-flight mass spectrometer is used to simultaneously monitor species produced in the supersonic expansion and allows correlation studies to be performed. Seven rotationally resolved vibronic bands have been measured near 400 nm, yielding spectroscopic constants for the $^2\Sigma$ ground and excited states. Vibronic isotope shifts, together with rotational line positions, permit the unambiguous determination of the spectral carrier and vibronic assignment. Since no *ab initio* studies for the CuSi molecule exist, a comparison to *ab initio* studies of the related NiSi molecule is presented. Time-of-flight mass spectrometric measurements indicate the facile formation of Cu_xSi_y clusters containing multiple copper atoms, in contrast to earlier mass spectrometric work on transition metal silicides. © *1995 American Institute of Physics.*

I. INTRODUCTION

Spectroscopic investigations of small metal-containing clusters have contributed significantly to our understanding of the bonding in metal–metal and metal–adsorbate systems. In the last decade, a wealth of experimental and theoretical data has been compiled, allowing a direct test of the theories used to model these quantized cluster systems.[1–3] As cluster size is increased, one expects the quantum properties of these systems to converge to bulk values. In this respect, detailed characterization of smaller systems in the gas phase should allow us to better understand some of the mechanisms responsible for bulk behavior. Clusters of intermediate size, as well as thin films, are likely to exhibit special properties which could be exploited in technological applications. In particular, clusters composed of metals and semiconductors are of immediate interest due to their common use in the construction of electronic devices. For example, aluminum is currently the element of choice for metallization in silicon integrated circuits due to its ease of processing, but has been shown to suffer from junction spiking and electromigration in submicron sized circuits. Copper has been proposed as an alternative, due to its lower resistivity (1.7 $\mu\Omega$ cm vs 2.65 $\mu\Omega$ cm for Al), but in this case, the possibility of the rapid diffusion of Cu into bulk silicon is of primary concern. For these reasons, several recent thin-film studies have focused on the interaction of Cu deposited on silicon substrates and subsequent copper silicide formation at the copper–silicon interface.[4–7] In these studies, the formation of various phases of copper silicides has been verified, even at deposition temperatures as low as 313 K.[7] The mechanisms responsible for the diffusion of copper into silicon for copper silicide formation is currently a topic of debate. Tu (Ref. 8) has suggested that the silicon lattice bonds are weakened by a shifting of electron density out of the Si–Si bonding orbital and into the metal–Si orbital. In the theoretical work of Hiraki,[9] an electrostatic screening mechanism is proposed, wherein the covalent silicon lattice bonds are effectively screened by the free electrons in the metal, weakening the silicon–silicon bonds and allowing the copper to diffuse into the lattice. In Hiraki's model, chemical interactions between individual copper atoms and the silicon lattice are considered unimportant, with the screening mechanism engaging only at a minimum copper film thickness.

In addition to the study of formation mechanisms, electrical properties at the metal–silicon interface have been correlated with the specific Cu_xSi_y stoichiometric phases present. One particular phase of copper silicide (the Cu_3Si eta phase) is believed to be primarily responsible for the electrical properties exhibited at the silicon–copper interface. The thin film studies of Aboelfotoh *et al.*, demonstrated that the presence of eta phase Cu_3Si catalyzed the oxidation of silicon to form a film of silicon and copper oxides which exhibited a nonmetallic resistivity (60 $\mu\Omega$ cm).[10] In another study, the Schottky-barrier behavior of Cu_3Si in *n*-type and *p*-type silicon has been investigated.[11] Because these bulk phase studies measure properties which are averages of local systems, specific information about the interactions between the individual metal and silicon atoms is not obtained. Another way to address the nature of the bonding occuring at the copper–silicon interface in bulk materials is through detailed gas phase studies of copper–silicon containing clusters, which constitutes the subject of this paper.

Although solid state spectroscopy and gas phase mass spectrometric studies of some copper silicides have been performed (see below), no gas phase spectroscopic data have been previously obtained. In an effort to characterize bonding properties of the ground and excited electronic states of metal silicides, we have combined cavity ringdown laser absorption spectroscopy (CRLAS) and time-of-flight mass spectroscopy (TOFMS) with a laser vaporization method for producing jet-cooled metal silicides. The presence of M_xSi_y species in a laser vaporization plasma reactor has been established with mass spectrometric measurements, and an exhaustive search for the electronic absorption spectra of these species has been carried out with the CRLAS apparatus. The results of this effort have yielded the first spectroscopic data for copper silicide clusters, as well as the first direct evidence

 0021-9606/95/102(13)/5190/10/$6.00 © 1995 American Institute of Physics
Downloaded 19 May 2006 to 131.215.225.175. Redistribution subject to AIP license or copyright, see http://jcp.aip.org/jcp/copyright.jsp

for the existence of any molecular metal silicide cluster containing more than a single metal atom. Experimental methods currently employed to obtain the optical spectra of metal containing clusters include resonant two-photon ionization (R2PI),[12] laser induced fluorescence (LIF),[13] photodepletion spectroscopy,[14] and cavity ringdown laser absorption spectroscopy (CRLAS).[15] Although highly sensitive and complimentary to the CRLAS method, the former techniques, commonly referred to as ''action'' techniques, rely on favorable dynamical events occurring in the molecule upon the absorption of a photon. In contrast, a direct absorption method such as CRLAS possesses the greatest degree of generality, and by comparison, only suffers from possible line broadening effects associated with short upper state lifetimes. However, to date, there is no evidence to suggest that detection of metal silicides with ''action'' techniques is impossible. Prior to our initial work in 1989,[15] direct absorption techniques had been effectively impossible to implement in this spectral region for the study of laser vaporized molecular beams, due to many factors. In this paper, we present the initial application of the CRLAS technique to the study of metal silicides with the first spectroscopic characterization of the gas phase CuSi molecule.

II. THEORETICAL STUDIES AND MOLECULAR ORBITAL CONSIDERATIONS

There currently exists very little theoretical literature on molecular metal silicide systems. Although topological bonding models have been proposed for larger metal silicides which were seen in mass spectrometric experiments (M=Cr, Cu, Mo, W),[16] these models are not applicable to the smaller clusters, which require detailed quantum mechanical treatments to accurately predict electronic state properties. To the best of our knowledge, only two molecular silicides, PdSi and NiSi, have been studied at the *ab initio* level.[17–19] Even though no *ab initio* studies have been carried out on CuSi, considerable insight can be inferred from the work on NiSi, owing to the approximate bonding similarities expected between Ni and Cu.

In the *ab initio* study by Shim and Gingerich,[18] all electron Hartree–Fock (HF), configuration interaction (CI), and multiconfiguration self-consistent field (MCSCF) calculations were applied to the NiSi molecule, yielding predictions for the ground and low lying excited electronic states. Atomic configurations considered for the ground state of NiSi combined the $3d^8 4s^2$ and $3d^9 4s^1$ configurations of the Ni atom with the $3s^2 3p^2$ configuration of Si. From these configurations, combinations of the ^3D and ^3F states of the Ni atom with the ^3P, ^1D, and ^1S states of the Si atom were considered. Similar to Ni_2 and NiCu, bonding in the NiSi molecule was predicted to occur only when the Ni atom was promoted from its atomic ground state ($3d^8 4s^2$) configuration to the $3d^9 4s^1$ level.[20,21] The resultant molecular ground state was predicted to have $^1\Sigma^+$ symmetry with σ and π bonds formed by combining the Ni $4s\sigma$ electron with the Si $3p\sigma$ electron and the Ni $3d\pi$ hole with the Si $3p\pi$ electron, respectively. In addition, 18 electronic states were predicted to lie within 1 eV of the ground state, due largely to the d-hole of the nickel atom. The equilibrium bond length predicted for the $^1\Sigma^+$ ground state was 2.228 Å, with a vibrational frequency of 313 cm^{-1} and a well depth of 1.07 eV. In the theoretical study of the NiSi molecule by Haberlandt,[19] similar results were obtained. Again, the ground state was predicted to be $^1\Sigma^+$, with an equilibrium bond length of 2.24 Å, a vibrational frequency of 303 cm^{-1}, and a binding energy of 1.89 eV. In addition to the ground state predictions, 10 electronic states were predicted within 1 eV of the ground state, again, due primarily to d-orbital promotions of the Ni atom. Unfortunately, no experimental data exist to support these predictions, although the experimental results of the present CuSi work are qualitatively in agreement with the predictions for NiSi.

A first order description of the ground state bonding in the CuSi diatom involves combining ground state Cu atoms ($3d^{10}4s^1$) with the $3s^2 3p^2$ configuration of Si. The reason for considering only the $3d^{10}4s^1$ configuration of the copper atom is justified by the fact that copper has been shown to readily form chemical bonds in this state (e.g., Cu_2, Cu_3, CuNi, CuAg, etc.).[2,21,22] In the Russell–Saunders coupling limit, this amounts to finding the states resulting from combining ^2S Cu atom with ^3P, ^1D, and ^1S states of the Si atom. States resulting from the combination of ^2S and ^3P terms (in order of increasing energy) are of $^2\Sigma$, $^2\Pi$, $^4\Sigma$, and $^4\Pi$ symmetry.[23] Similarly, possible states resulting from the ^2S and ^1D combination possess $^2\Sigma$, $^2\Pi$, and $^2\Delta$ symmetry, while those resulting from the addition of ^2S and ^1S atomic states produce only a $^2\Sigma$ state. Since the ground state of Si is ^3P, it is apparent that the most likely candidate for the ground state of the CuSi molecule is a state of $^2\Sigma$ symmetry, with the chemical bonding composed primarily of a single σ bond. This would suggest that the bond length and vibrational frequency of CuSi should be similar to those predicted for the NiSi diatom.[18,19] These intuitive models are supported by the molecular constants extracted in this spectroscopic study and will be discussed in more detail later in this paper.

III. EXPERIMENT

A. Cavity ringdown laser absorption spectroscopy

In the pulsed cavity ringdown technique, first developed by O'Keefe and Deacon in 1987 for the determination of mirror reflectivities,[24] molecular absorption is deconvoluted from the measured photon decay time of a high finesse optical cavity which is injected with short pulses of laser light. The high sensitivity of this technique was demonstrated by measuring doubly forbidden transitions in molecular oxygen. Since our first application of the cavity ringdown technique to the study of pulsed molecular beams,[15] several other groups[25,26] have employed the technique for various purposes, including adaptation to kinetics studies[27] and the spectroscopy of OH in flames.[28]

In the simplest picture of the CRLAS technique, a two mirror cavity is injected with a pulse of narrow band laser light with a coherence length shorter than the mirror spacing. The trapped light makes many traversals of the cavity, with a small fraction of the light transmitting through the exit mirror with each pass. The intensity of the transmitted light at the exit mirror is monitored with a photomultiplier, which

Downloaded¬19¬May¬2006¬to¬131.215.225.175. Redistribution¬subject¬to¬AIP¬license¬or¬copyright,¬see¬http://jcp.aip.org/jcp/copyright.jsp

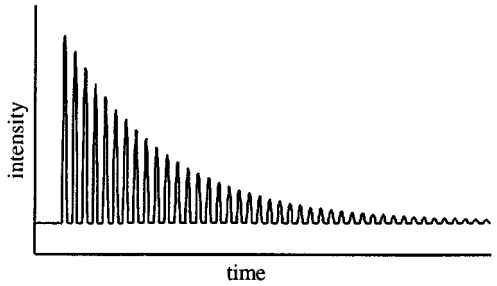

FIG. 1. In the short pulse limit, discrete pulses of light spaced $2L/c$ apart exit the cavity. The peak intensities of the successive pulses are fit to a first order exponential. Typical ringdown decays consist of ten thousand such pulses.

sees a series of pulses of decreasing intensity spaced in time by the round trip time $(2L/c)$ of the cavity, as depicted in Fig. 1. Because the amount of light which transmits through the exit mirror is linearly proportional to the amount of light still trapped inside the cavity, the intensity decay envelope of the successive peaks follows a simple first order exponential expression

$$I(t)=I_0e^{(-Tt2L/c)}, \tag{1}$$

where T is the transmission coefficient of the cavity, L is the cavity mirror spacing, and t is time. Measurement of the cavity ''ringdown'' time (t, wherein $I=I_0e^{-1}$) allows the transmissivity of (or absorption inside) the cavity to be determined, if the mirror spacing (cavity length) is known. This cavity ''transmissivity'' represents the total losses experienced by the light pulse while traversing the cavity, including mirror transmissivity, optical scattering, mirror coating absorption, and molecular absorption for species located between the two mirrors. Measurement of the cavity ''ringdown time'' at a given wavelength gives a direct measurement of the total losses experienced by the circulating light over a single cavity round trip pass. A plot of cavity losses vs wavelength allows an absorption spectrum to be obtained for species placed in the cavity. Accurate relative absorption intensities for molecular transitions (in the limit of weak absorption) are readily determined by comparing cavity losses with and without the sample present.

Because each laser pulse constitutes an independent measurement of the ringdown time, the CRLAS technique is relatively insensitive to the large power fluctuations exhibited by pulsed dye lasers. Additionally, extremely high levels of sensitivity can be achieved with a relatively lenient constraint on how precisely the decay time is determined. In practice, higher mirror reflectivity leads to a higher achievable sensitivity, due to the fact that the fractional error in the ringdown time decreases with increased reflectivity. In Table I, the sensitivity of the CRLAS technique is calculated for different mirror reflectivities for various degrees of uncertainty in the measured ringdown decay time. Typically, the highly reflective mirrors have a usable bandwidth of approximately $\pm 10\%$ of the wavelength at their maximum reflectivity. From this table, it is evident that mirror reflectivity and precision in the measurement of the ringdown time combine to dictate the theoretical sensitivity in CRLAS, with a fractional absorption of better than 1 ppm easily realized. It is important to note, however, that in these molecular beam studies, the theoretical sensitivity limit of our present apparatus ($\sim 5\times 10^{-8}$ fractional absorption) is not realized primarily because of the optical scattering encountered by the circulating laser light in the dense laser vaporized plasma. It is also worth noting that with the laser power (3 mJ) used in these studies, we are still many orders of magnitude away from the shot noise limit, contrary to conclusions implied in a recent study.[25] This is easily shown by considering the uncertainty associated with a single pulse of light (see Fig. 1) as it exits the cavity and impinges on the photomultiplier. For our excimer-pumped dye laser (Lumonics 864T+Lambda FL3002E), a 15 ns pulse consisting of $\sim 10^{16}$ photons is produced, with 10^8 photons reaching the detector in the first pass through the cavity. At the cavity ringdown time, $\sim 3\times 10^7$ photons strike the detector in 15 ns, leading to a shot noise limit of $\sim 5\times 10^{-3}$ in the last pulse as it exits the cavity. Because the measurement of the ringdown time consists of thousands of such pulses, this small uncertainty in the *amplitude* of a single pulse is insignificant to the overall precision of the ringdown *time* determination. Shot noise would only limit sensitivity in the case where extremely low power lasers (submicrojoule) were used.

Because the CRLAS technique is a direct absorption method and therefore governed by Beer's law, high cluster densities in the probe region are desirable. Hence, the signal to noise ratio obtained in these studies is limited principally by the ability to produce the desired cluster vs the tendency to form very large clusters which are more likely to scatter light in a nonresonant process such as Rayleigh scattering. Because the process of Rayleigh scattering scales as the

TABLE I. Theoretical sensitivity limits for the CRLAS technique as a function of mirror reflectivity and ringdown time determination. Because measurement of the decay time only allows determination of the total cavity losses, the ability to discriminate background mirror losses from sample absorption sets an upper limit to the technique sensitivity. This ability is limited by the precision and accuracy of the cavity ringdown time measurement.

Mirror reflectivity	No. of passes to e^{-1}	Time constant to 1%	Time constant to 2%	Time constant to 3%	Time constant to 10%
0.995 0	100	$\pm 5.05\times 10^{-5}$	$\pm 1.02\times 10^{-4}$	$\pm 1.5\times 10^{-4}$	$\pm 5.5\times 10^{-4}$
0.999 0	500	1.1×10^{-5}	2.04×10^{-5}	3.0×10^{-5}	1.1×10^{-4}
0.999 5	1 000	5.05×10^{-5}	1.02×10^{-5}	1.5×10^{-5}	5.5×10^{-5}
0.999 9	5 000	1.1×10^{-6}	2.04×10^{-6}	3.0×10^{-6}	1.1×10^{-5}
0.999 95	10 000	5.05×10^{-7}	1.02×10^{-6}	1.5×10^{-6}	5.5×10^{-6}
0.999 99	50 000	1.1×10^{-7}	2.04×10^{-7}	3.0×10^{-7}	1.1×10^{-6}

Downloaded¬19¬May¬2006¬to¬131.215.225.175. Redistribution¬subject¬to¬AIP¬license¬or¬copyright,¬see¬http://jcp.aip.org/jcp/copyright.jsp

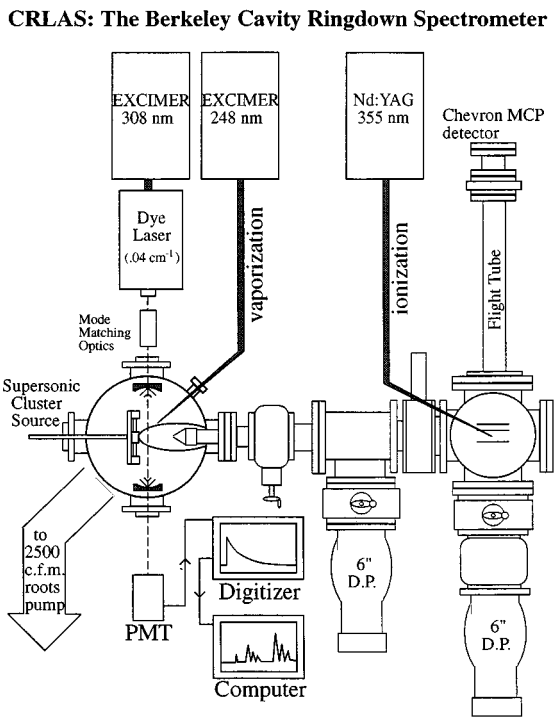

FIG. 2. Berkeley CRLAS/TOFMS apparatus. A laser vaporized pulsed molecular beam of metal clusters is generated in a vacuum chamber and perpendicularly intersected by the laser pulse train. The ringdown decay is timed to coincide with the transient molecular beam and is monitored with a photomultiplier. The decay waveform is digitized and transferred to a PC for calculation of the molecular absorption at each laser wavelength. Neutral species in the molecular beam are monitored with a differentially pumped time of flight mass spectrometer. The design allows *in situ* mass spectrometric measurements to be made while monitoring absorption spectra.

fourth power of the frequency,[29] background source "noise" is substantially worse at shorter wavelengths, as in the present study. A critical review of the CRLAS technique in its past and current forms, with emphasis on sensitivity considerations and possible future configurations is beyond the scope of this paper but is presented in a forthcoming review.[30]

The Berkeley cavity ringdown laser absorption spectrometer and time-of-flight mass spectrometer (TOFMS) are diagrammed in Fig. 2. The experimental design incorporates three stages of differential pumping, consisting of a main source chamber evacuated by a large Roots pump (2500 cfm Edwards EH4200), and two regions pumped by small diffusion pumps (Varian VHS6). Each of the three regions are separated by electroformed molecular beam skimmers each having a 2 mm orifice (Beam Dynamics). The CRLAS experiment is performed in the source chamber, where an average background pressure of 50 mTorr is maintained with the molecular beam operating at 20 Hz. Background pressure in the ionization region of the TOFMS is maintained at $\sim 5\times 10^{-7}$ Torr. This tandem design allows in-situ mass spectrometric characterization of the supersonic molecular beam while simultaneously obtaining absorption spectra with the CRLAS spectrometer.

Copper silicide cluster production is achieved by laser vaporization of a copper rod in a modified Smalley-type source.[31] Approximately 200 mJ of 248 nm excimer laser light (Questek model vβ) is focused through the exit slit of a fan-shaped nozzle (tapered to a 2 mm hole) to a 1 mm spot onto a continuously rotating and translating Cu rod, while a pulse of He carrier gas (120 psi) seeded with $\sim$0.2% silane passes over the vaporization region. Cylinders of varying silane concentration, ranging from 2% to 0.2%, were prepared to quantitatively study concentration effects on cluster production. The vaporization and dehydrogenation processes produce bare metal clusters, metal silicides, and pure silicon clusters which cool as they expand into the evacuated chamber. The relative abundances of the species produced are monitored with the mass spectrometer and found to be extremely sensitive to source parameters and silane concentration in the carrier gas. Maximum copper silicide production is achieved for a plasma which is largely invisible to the naked eye, while a decrease of the silane content in the gas mixture returns the copper plasma to its characteristic bright green color. One to three nozzle diameters downstream of the source exit slit, the molecular beam is intersected perpendicularly by the ringdown laser pulse train at the center of the two mirror cavity.

Proper timing of the ringdown laser pulse with respect to the transient molecular beam assures maximum temporal overlap between the two events. In fact, one of the primary advantages of employing CRLAS for pulsed molecular beams is the similar time scales of both the molecular beam and ringdown events (5–25 μs), allowing a probe duty cycle near unity to be achieved. The injected laser pulse consists of a few mJ of narrow band (0.04 cm^{-1}) excimer pumped dye laser light, the TEM_{00} component of which is coupled to the cavity with the use of a simple telescope. Roughly 1 part in 10^8 of this light passes through the exit mirror of the cavity and is detected with a photomultiplier (Hammamatsu R912). Because the coherence length of the injection laser is short compared to the 0.5 m mirror spacing (a 0.04 cm^{-1} bandwidth gives a $\sim$4 cm coherence length) and the intensity variation of the input pulse is erratic, longitudinal mode competition in the cavity is essentially random,[32] with no étalon effects seen at the photomultiplier. This fact means that our first-order picture of the ringdown decay is applicable, i.e., the light trapped in the cavity is essentially particlelike and undergoes a first-order exponential decay. The resultant ringdown decay waveform is amplified, digitized with a 12-bit, 20 MHz transient digitizer, and sent to a computer for analysis. Typically, 16 laser shots are averaged per wavelength in order to reduce noise introduced by fluctuations in the pulsed molecular beam. In these studies, two sets of highly reflective dielectric mirrors with a 6 m radius of curvature are used to cover the UV–VIS region (420–380 nm). In the data presented here, base line variation of the mirror reflectivities is subtracted, and molecular absorption is plotted per single pass.

B. Time-of-flight mass spectrometer

Coupled to our CRLAS apparatus is a Wiley–Mclaren[33] type time-of-flight mass spectrometer (TOFMS). Photoionization of the neutrals in the last pumping stage is achieved in these copper silicide studies with the unfocused third har-

Downloaded¬19¬May¬2006¬to¬131.215.225.175. Redistribution¬subject¬to¬AIP¬license¬or¬copyright,¬see¬http://jcp.aip.org/jcp/copyright.jsp

monic (355 nm) output of a pulsed Nd:YAG laser (Continuum NY61) operating at 20 Hz. The resultant cations are extracted at right angles to the molecular beam and accelerated to 4 keV. A pair of variable voltage deflectors are used to cancel the beam energy and an Einzel lens is employed to enhance focusing of the ions onto 2 in. dual microchannel plates (Galileo #40/25) located at the end of a 1.3 m field free flight tube. The microchannel plate ion optics incorporate a special impedance-matched 50Ω anode assembly which minimizes ringing.[34] The output of the MCP assembly is fed directly into a 500 Msample/s, 500 MHz input bandwidth digital storage oscilloscope (Tektronix TDS524A). The resultant time-of-flight spectrum is transferred to a computer for calibration and calculation of molecular masses. Mass resolution of the system is 350, allowing the various isotopic combinations of the copper containing clusters to be resolved. This tandem design allows characterization of the molecular beam under a variety of source conditions, and greatly aids in maximizing cluster concentrations. In addition, correlation studies can be performed by simultaneously monitoring direct absorption and mass spectra. This procedure is particularly useful in identifying oxide and nitride spectral carriers in rapid low resolution CRLAS scans. For example, the addition of trace amounts of O_2 and N_2 to our carrier gas produces large increases in the abundances of metal oxides and nitrides, as well as the intensities of the associated CRLAS spectra. Similarly, monitoring mass spectra while varying silane addition indicates whether a particular unknown absorption feature contains silicon (or possibly hydrogen). Although photofragmentation of cluster photoions can hamper these studies, we have found them to yield qualitatively reliable means of eliminating certain species as carriers when unresolved, diffuse absorption spectra are obtained. In the present study, the mass spectrometer was initially used to determine the presence of both copper and silicon in the spectral carrier. This was done by vaporizing different metals in the presence of various gas mixtures. These qualitative studies were later confirmed by direct assignment of the spectroscopic signature evident in the absorption spectra. The frequencies of CRLAS spectra in these copper silicide studies were calibrated with the well-known spectra of SiH (Ref. 35) and Si_2 (Ref. 36) that occur in this spectral region.

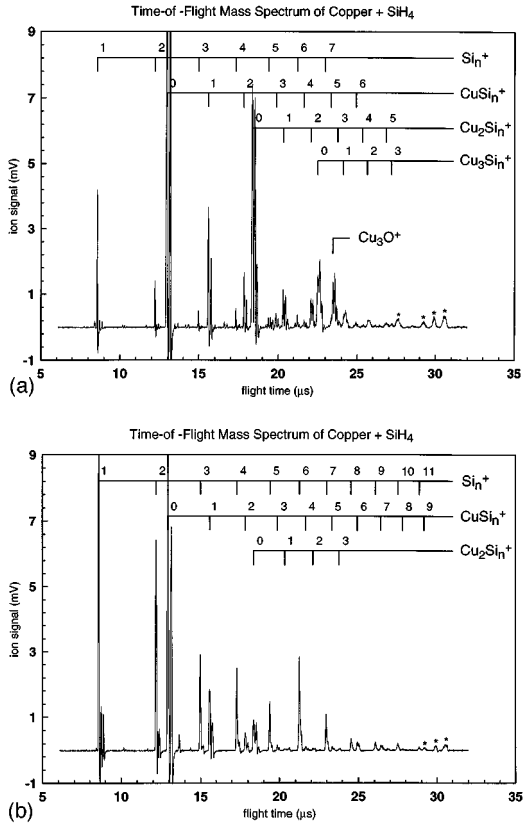

FIG. 3. (a),(b) TOFMS of jet-cooled copper silicides formed in a laser vaporization plasma reactor, where the effects of silane concentration on cluster production is displayed. In (a), a silane concentration of 0.2% (He balance) is used, leading to metal silicide formation. In (b), the silane concentration is increased to 1%, almost eliminating the metal containing species in favor of the production of pure silicon clusters. In both cases, vaporization energy, carrier gas pressure, and photoionization (355 nm) conditions are identical. The peaks labeled with asterisks are due to photoionization of residual hydrocarbons present in the ionization region.

IV. RESULTS AND DISCUSSION

A. Copper silicides: TOFMS

Copper silicide molecular beam studies were first carried out in the mass spectrometric experiments of Beck.[37,38] In that work, metal silicides of chromium, tungsten, molybdenum, and copper were produced in a supersonic expansion and probed with a time-of-flight mass spectrometer employing 157 nm or 193 nm photoionization. Copper silicides were produced using one of three different methods. The first employed a Smalley-type laser vaporization source wherein laser ablated silicon was entrained in a He carrier gas which was seeded with a volatile copper carbonyl compound. The second method involved vaporization of a silicon rod which had a thin layer of copper vacuum deposited upon it in a crosshatch pattern. The final method, which yielded the best copper silicide signals, involved vaporization of a copper rod in the presence of a He carrier gas seeded with trace amounts of silane (which were not specified). Dehydrogenation of the silane in the metal plasma produced free silicon which then reacted in the throat of the source nozzle to produce clusters. Dominant clusters detected in this study consisted of Cu_xSi_y containing only a single copper atom, and between six and sixteen silicon atoms. In fact, no species with $x>1$ or $y<6$ were observed at all. Photoionization laser wavelength and fluence dependencies suggested that the metal silicide species did not undergo significant photofragmentation, in contrast to the known fragmentation of pure silicon cluster ions, indicating that the lack of species with $x>1$ was not a result of fragmentation of larger clusters. Beck interpreted these results as a manifestation of the ability of a single copper atom to react with a large number of silicon atoms. Since that work, theories have been proposed to explain Beck's findings based on qualitative bonding models, suggesting that highly symmetric polyhedral clusters are formed.[16]

Time-of-flight mass spectra of copper silicides produced in our silane-seeded laser vaporization plasma reactor source are shown in Figs. 3(a) and 3(b), where the effect of silane

Downloaded¬19¬May¬2006¬to¬131.215.225.175. Redistribution¬subject¬to¬AIP¬license¬or¬copyright,¬see¬http://jcp.aip.org/jcp/copyright.jsp

concentration on cluster production is exhibited. In contrast to the results of Beck's work, we observe Cu_xSi_y species containing up to three copper atoms and as many as nine silicon atoms. Moreover, we also observe copper silicide clusters with fewer than six silicon atoms in high abundance, again in contrast to Beck's findings. Because the distribution of species evident in a mass spectrometric study will involve a convolution of source conditions, ionization cross sections, and possible photofragmentation dynamics, it is difficult to quantitatively explain the differences between experiments performed in different laboratories, especially when different photoionization wavelengths are employed. However, some qualitative conclusions can be drawn by comparing the mass spectra in Figs. 3(a) and 3(b) with those obtained by Beck. In Fig. 3(a), a silane concentration of ~0.2% (He balance) is found to produce substantially more copper-containing species than those of Fig. 3(b), where the silane concentration has been increased to ~1%. Similarly, pure silicon species are increased in the case of high silane concentration, under the same source conditions. More importantly, the ratio of Cu_xSi_y to Si_n species as a function of silane concentration suggests that the amount of copper vaporized is reduced by the addition of silane. This result would follow if dehydrogenation of silane actually degrades the average energy in the laser generated plasma which would otherwise be available for the atomization of copper. This possibility is supported by the change in the visual appearance of the metal silicide plasma as a function of silane concentration. As the silane concentration is increased, the normally bright green plasma becomes increasingly invisible, indicating a quenching in the vaporization region. If this were the case it would follow that, in the work of Beck, silane concentrations were so high as to prevent the efficient atomization of the copper, leading to copper silicides with only a single copper atom present. In fact, for all of the metals studied in that work, only a single metal atom is evident in all of the metal silicides produced. From these considerations, it appears that source conditions in the previous work are responsible for the cluster distributions produced, not a geometrical stabilization of preferred stoichiometries as postulated by some theoreticians (e.g., Ref. 16).

Even if our metal silicide TOFMS spectra were distorted by photofragmentation processes, this would indicate the presence of even larger Cu_xSi_y species which, again, contain more than a single metal atom in the parent cluster. From our mass spectrometric data, it is clear that copper silicides of various stoichiometries are readily produced in our plasma reactor source, giving conclusive evidence for the existence of molecular metal silicides which contain several metal atoms. These results are important in the context of the solid phase studies, which suggest special properties for the different stoichiometric phases of metal silicides at the metal–silicon interface.[4–7] Another interesting feature evident in our mass spectra [Fig. 3(a)] is the exceptionally large mass peak corresponding to the metal oxide Cu_3O. This peak is extremely small in our mass spectra of pure copper clusters generated in helium buffers, suggesting a possible catalytic mechanism involving silicon atoms or clusters. In the absorption spectra of CuSi presented in the following section, conditions which favored metal silicide production (both CuSi and larger Cu–silicides) also produced more intense absorption spectra for the CuSi diatom, as expected. These points underscore the sensitive role which source conditions play in generation of clusters and the subsequent limitations imposed on the interpretation of mass spectra.

B. Electronic absorption spectra

Cavity ringdown rovibronic spectra of the $B\Sigma - X\Sigma$ system of CuSi were obtained in the UV–VIS region extending from 410 to 380 nm and consist of a single vibronic progression in the upper electronic state. Low and high resolution (0.3 cm^{-1} and 0.04 cm^{-1}, respectively) spectral scans were performed with a pulsed dye laser operating on BBQ and PBBO dyes mixed in *p*-dioxane. We adopt the *B* label for the upper electronic state based on the fact that our electronic origin is too high in energy to correspond to the first excited state asymptotes of either the copper or silicon atom, taking into account estimated upper and lower state well depths. Although we have measured absorption features farther to the red, which, again, are only present under conditions which favor copper silicide production, we have not yet been able to definitively assign them to the CuSi diatom, due to the lower signal to noise ratio of those spectra.

In the $B-X$ ''blue'' band system presented in this paper, a total of eight vibronic bands have been obtained, seven of which exhibit measurable vibrational isotope shifts. The bandhead frequencies of the lighter isotope ($^{63}Cu^{28}Si$) were fit to the standard expression

$$\nu = \nu_0 + \omega'_\epsilon(v' + 1/2) + \omega'_\epsilon\chi'_\epsilon(v' + 1/2)^2, \tag{2}$$

where ν_0 represents the transition energy from the lowest vibrational level of the lower electronic state to the bottom of the upper electronic well. Although attempts were made to increase population in the excited vibrational levels of the ground electronic state (decreasing gas pressure, increasing vaporization energy, etc.), no hotband spectra were obtained, presumably due to the efficient vibrational cooling that is obtained in the expansion. High resolution scans yielded rotationally resolved spectra, allowing determination of the rotational constants and associated bond lengths of the ground and upper electronic states. Accurate determination of the vibronic assignment in the upper state as well as confirmation of the spectral carrier was facilitated with the measured isotope shifts.

C. Vibronic isotope shifts

In the harmonic approximation, the vibrational frequency of a diatomic molecule is dictated by the square root of the ratio of the force constant to the reduced mass. Therefore, the ratio of the vibrational frequencies of any given pair of isotopes uniquely determines the quantity ρ, which is the square root of the ratio of the reduced masses. Extending this concept to include anharmonic terms,[39] the vibrational term values expected for the heavier isotope in a given electronic well are given by

Downloaded¬19¬May¬2006¬to¬131.215.225.175. Redistribution¬subject¬to¬AIP¬license¬or¬copyright,¬see¬http://jcp.aip.org/jcp/copyright.jsp

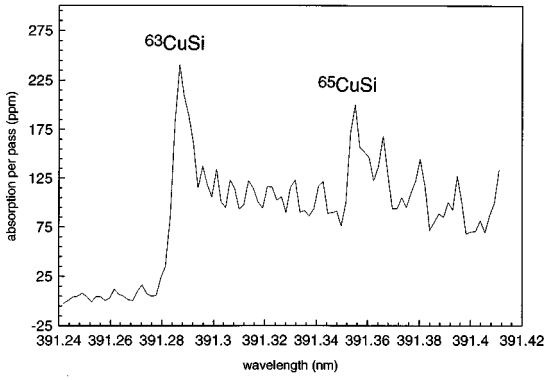

FIG. 4. Low resolution scan ($\sim$0.3 cm^{-1}) of the 4-0 vibronic band of the $B\ ^2\Sigma - X\ ^2\Sigma$ system of CuSi. In this scan, the two most abundant isotopes of the CuSi molecule lead to two prominant bandheads. Analysis of the observed splitting for each vibronic band allows an unambiguous assignment.

$$G^{(i)} = \rho\omega_\epsilon(v+1/2) - \rho^2\omega_\epsilon\chi_\epsilon(v+1/2)^2 + \rho^3\omega_\epsilon\gamma_\epsilon(v+1/2)^3 - \cdots, \quad (3)$$

where v is the vibrational quantum number and $\omega_\epsilon\chi_\epsilon$ and $\omega_\epsilon\gamma_\epsilon$ are anharmonic constants. Keeping terms only through ρ^2 and labeling upper and lower electronic states with $'$ and $''$, the predicted isotope shift for transitions out of the ground vibrational level of the lower electronic state is

$$\Delta\nu = \nu - \nu^{(i)} = (1-\rho)\omega'_\epsilon(v'+1/2) - (1-\rho^2)\omega'_\epsilon\chi'_\epsilon(v'+1/2)^2 - [(1-\rho)\omega''_\epsilon/2 - (1-\rho^2)\omega''_\epsilon\chi''_\epsilon/4], \quad (4)$$

where $\nu^{(i)}$ is the vibronic band energy of the heavier isotope. From the above expression, it is evident that the magnitude of the observed isotope shifts will be determined from the upper and lower state molecular constants and vibronic assignments. Comparison of predicted splittings based on measured molecular constants allows a direct test of a given vibronic assignment, for a given ρ. Using the values ω'_ϵ and $\omega'_\epsilon\chi'_\epsilon$ obtained from the upper state vibrational fit, the isotope shifts (excluding the term in brackets) can be predicted. At this point, it is worth noting that even though the lower state vibrational frequency is not directly measured in these studies, it can be inferred from the determination of the term in brackets, which is the zero point isotope splitting of the lower electronic state. This is accomplished by plotting the predicted isotope shifts for a given vibronic assignment vs the measured values and varying the assignment until a slope near unity is achieved. When this is done, the y-intercept determines the zero point splitting of the ground state. Excluding the anharmonic term, the ground state vibrational frequency can then be calculated with reasonable accuracy, assuming that the anharmonic contribution is small.

Typical low resolution CRLAS spectra of the $B-X$ system of CuSi are shown in Fig. 4, where the 4-0 vibronic band is shown. Evident in the 4-0 band is a double bandhead signature which is also is seen in seven of the eight vibronic bands obtained in this study. This bandhead spacing is a manifestation of the two naturally abundant isotopic CuSi species, with a regular increase in the bandhead spacing extending towards the blue. From the two naturally abundant

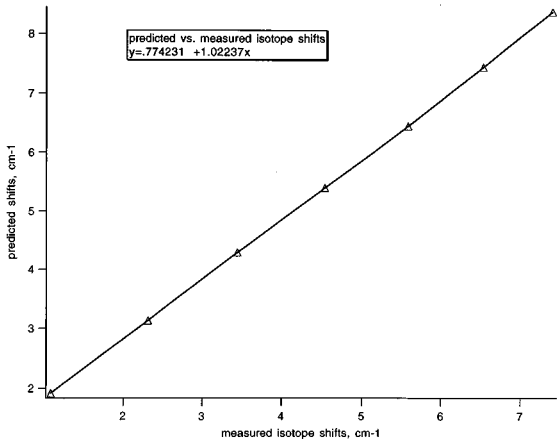

FIG. 5. A plot of predicted vs measured isotope splittings serves as a check of a given vibronic assignment. When the slope of the graph is unity, the y-intercept represents the splitting associated with the zero point isotope splitting of the ground electronic state. From this value, the vibrational frequency of the ground electronic state can be estimated.

isotopes of the copper atom (^{63}Cu:^{65}Cu=69:31) and the single dominant isotope of the silicon atom (^{28}Si:^{29}Si:^{30}Si =92:5:3), two isotopomers (^{63}Cu^{28}Si and ^{65}Cu^{28}Si) are expected to dominate the observed spectra. In fact, with our current signal to noise ratio we are not able to discern features due to the less abundant isotopic species of silicon. Therefore, for the two most abundant molecular isotopes, ρ=0.995 254.

Using the values obtained from the vibrational fit for the upper state (see Table III), the predicted isotope shifts, including the constant zero point term, were calculated for different upper state vibrational assignments. The results of the best fit are shown in Fig. 5, wherein the predicted shifts are plotted against the measured values. From this analysis, wherein a slope of nearly unity is obtained, we conclude that the spectral carrier is in fact CuSi, with the corresponding vibronic assignment as given in Table II. Using the y-intercept obtained from the fit of Fig. 5 and ignoring anharmonicity in the lower state, the lower state vibrational frequency can be calculated. Rigorously, the origins of the bands for the two different isotopes would be used for the measured isotope shifts, instead of the bandhead positions. Because of spectral congestion in the rotationally resolved bands, this was not possible and therefore introduces a small systematic error to the measured values obtained in this study. This fact, together with neglecting the possibility of a

TABLE II. Bandhead positions for the $B-X$ vibronic system of CuSi.

Assignment ($v'-v''$)	Bandhead (cm^{-1})
0-0	24 502.5
1-0	24 774.1
2-0	25 041.5
3-0	25 302.7
4-0	25 556.8
5-0	25 807.1
6-0	26 051.2
7-0	26 289.7

Downloaded¬19¬May¬2006¬to¬131.215.225.175. Redistribution¬subject¬to¬AIP¬license¬or¬copyright,¬see¬http://jcp.aip.org/jcp/copyright.jsp

TABLE III. Molecular constants for the $B-X$ system of CuSi.[a]

	$X\ ^2\Sigma$	$B\ ^2\Sigma$
ν_{00}		24 501.6
B_e	$B_0=0.164\ 80(21)$	0.129 5(5)
r_e (Å)	(r_0) 2.298	2.60
α_e	na	0.002 1(5)
$D_e\times10^7$	(D_0) 1.64 (est)	1.12 (est)
ω_e	330(15)	277.92(4)
$\omega_e\chi_e$	na	2.818

[a]Unless indicated, all constants are given in cm^{-1}.

large lower state anharmonicity, introduces conservatively large error bars to the calculated lower state vibrational frequency, as indicated in Table III. Only with the direct measurement of vibrational hot bands could accurate values for ω_ϵ'' and $\omega_\epsilon''\chi_\epsilon''$ be obtained. However, the value of ω_ϵ'' obtained in this fashion, when compared to the rotational constants presented later, is found to be consistent with Badger's rule, viz., $r_\epsilon^2\propto\omega_\epsilon^{-1}$.

D. Rotational analysis

Of the eight vibronic bands measured, two have been rotationally analyzed to yield rotational constants for the ground and excited electronic states of the lighter isotope. From molecular orbital considerations discussed earlier combined with the fact that the observed spectra exhibited no Q-branches, the bands were fit as $^2\Sigma-{}^2\Sigma$ transitions. Term values for the two spin–rotation states are given by the expressions

$$F_1=B_vN(N+1)+\gamma N/2+\text{distortion terms}$$

and

$$F_2=B_vN(N+1)-\gamma(N+1)/2+\text{distortion terms}, \qquad (5)$$

where B_v is the rotational constant for a given vibrational level, N is the rotational quantum number, and γ is the spin–rotation constant, which is typically much less than B_v and may be positive or negative.[40] The resulting rovibronic band structure is shown in Fig. 6 and consists of six branches, including two R-branches, two P-branches, and two very weak ''satellite'' Q-branches. The signature of such a band system will be a splitting of each of the rotational lines into a doublet, the splitting of which will increase linearly with N. In our case, due to the limited bandwidth of our probe laser (0.04 cm^{-1}), this splitting is not expected to become resolved, except for very high N, where a broadening of the lines might become apparent. For this reason, in the fits that follow, the constant γ is set equal to zero. This leads to a band system which essentially looks the same as a $^1\Sigma-{}^1\Sigma$ system. Similarly, attempts to include the distortion constant D_e in the fits that follow led to either negative distortion constants or values with unacceptable uncertainties. The reason for this is easily seen when the Kratzer relation[41] is employed to estimate the magnitude of D_e,

$$D_e=4B_e^3/\omega_\epsilon^2. \qquad (6)$$

For the upper electronic state, using the experimentally determined constants in Table III, this leads to an estimate of $D_e\cong1.15\times10^{-7}$ cm^{-1}, which, even for $N=20$, leads to a correction of only ~0.02 cm^{-1}, or roughly 1/2 of our laser bandwidth. For this reason, estimates of D_e' and D_e'' in the table are derived using the Kratzer relation, while these terms were set equal to zero in the rotational fits. Setting distortion constants in the fits to the estimated values produced insignificant changes to the constants otherwise obtained and are therefore not included. Figure 7 shows the rotationally resolved spectra of the 1-0 band with the rotational assignment as indicated. The bandhead due to the heavier isotope ^{65}CuSi is indicated with an arrow. One feature common to all of the observed bands is the rapid bandhead formation in the R-branch, consistent with a large decrease in vibrational frequency and increase in bond length upon excitation into the upper electronic state. Line positions for the two fitted bands (1-0 and 2-0) are available from the authors. The derived constants are listed in Table III. Because no transitions were

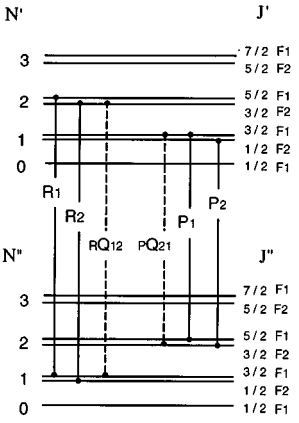

FIG. 6. Detail of the six possible rotational branches of a $^2\Sigma-{}^2\Sigma$ band. The signature of such a system is a splitting of each rotational line which increases linearly with N, the rotational quantum number. Because the splitting is not resolved in this scan, the band fits equally well to a $^1\Sigma-{}^1\Sigma$ system.

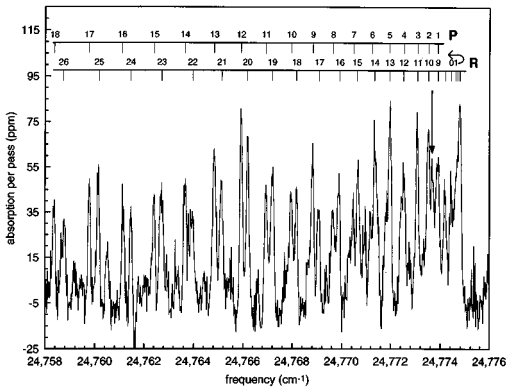

FIG. 7. Rotationally resolved CRLAS spectra of the 1-0 vibronic band of the $B-X$ system of CuSi, with the assignment as indicated. The bandhead due to the heavier isotope (65CuSi) is indicated with an arrow. In this scan, 16 laser shots are averaged per wavelength point, with a step size of $\sim1/3$ that of the 0.04 cm^{-1} laser bandwidth. Total acquisition time for this 18 cm^{-1} scan is 15 min.

Downloaded¬19¬May¬2006¬to¬131.215.225.175. Redistribution¬subject¬to¬AIP¬license¬or¬copyright,¬see¬http://jcp.aip.org/jcp/copyright.jsp

measured out of excited vibrational levels of the ground vibrational state, α_e'' could not be determined. Using the constants obtained in the vibrational fit of the upper state, the corresponding well depth can be qualitatively estimated with the relation (for Morse oscillators)

$$D^e = \omega_\epsilon^2 / 4\omega_\epsilon \chi_\epsilon . \tag{7}$$

Comparison of the experimentally determined molecular constants of CuSi with those predicted for NiSi in the *ab initio* study of Shim and Gingerich[18] and Haberlandt[19] provide a consistent picture of the bonding in these two transition metal silicides. In both species, bonding between the metal and silicon atom is primarily of $s\sigma$ character, as expected for a copper compound. Using the predicted bond length for NiSi from Ref. 18, a rotational constant for NiSi of 0.18 cm^{-1} would be expected for the ground state, slightly larger than the 0.165 cm^{-1} constant experimentally determined for CuSi. This result suggests the copper species is less tightly bound than the nickel species, implying a small additional bonding contribution from the open Ni *d*-orbital.

Finally, the experimentally determined ground state CuSi dissociation energy of 2.36 eV (Ref. 42) is consistent with the value one might estimate from this experimental work, based on a comparison of the 278 cm^{-1} upper state frequency (and 0.849 eV well depth) vs the 330 cm^{-1} lower state frequency. This 2.36 eV value, however, is substantially smaller than the experimentally determined dissociation energy of NiSi, which was found to be 3.26(17) eV.[43] In contrast, the predicted binding energies for NiSi of Ref. 19 (1.89 eV) and Ref. 18 (1.13 eV) are both substantially smaller than the experimental value obtained in the above referenced mass spectrometric work. Resolution of these discrepancies requires detailed ground state information for both NiSi and CuSi. This comparison of well depth, therefore, is quite approximate due to the lack of lower state information obtained in this experimental work. Direct measurement of the lower state vibrational frequency and anharmonicity would obviously facilitate these comparisons. Comparison of the vibrational frequency of CuSi with the experimentally determined frequency for the AuSi diatom (391 cm^{-1}) (Ref. 44) underscores the importance of the *d*-orbital contributions to overall bonding as one proceeds down the Periodic Table.[3] Consistent with the larger vibrational frequency, the binding energy of AuSi (3.3 eV) (Ref. 45) is substantially larger than either NiSi or CuSi.

V. SUMMARY

The first gas phase spectrum of copper silicide has been obtained with the CRLAS technique, employing a laser vaporization plasma reactor source. Rovibronic spectra have been fit to yield molecular constants for the ground and excited $^2\Sigma$ states. Measured vibronic isotope shifts have allowed definitive assignment of the progressions observed in the upper electronic state and have verified the spectral carrier as CuSi. In addition to the absorption spectra obtained in this initial application of CRLAS to the study of metal silicides, time-of-flight mass spectra have been presented which conclusively demonstrate for the first time the existence of molecular silicide species containing multiple copper atoms, in direct contrast to the earlier experimental results of Beck. This has important implications for solid state findings and future work. In the case of CuSi, this study suggests the spontaneous formation of copper silicides from ground state copper and silicon atoms, consistent with the appearance of silicide formation in low annealing temperature (~300 K) solid state experiments. Comparison of these CuSi experimental results with the *ab initio* studies of NiSi indicate the similarities of the chemical bonds formed between the two metal and silicon species, and underscore the need for more experimental and theoretical work on these important systems.

ACKNOWLEDGMENTS

This work was supported by the Air Force Office of Scientific Research (Grant No. F49620-93-1-0278). Equipment was provided by the National Science Foundation (Grant No. CHE-9123335). J. J. Scherer thanks IBM for a predoctoral fellowship awarded during part of this research work.

[1] M. M. Kappes, Chem. Rev. **88**, 369 (1988).
[2] M. D. Morse, Chem. Rev. **86**, 1049 (1986).
[3] See, e.g., S. P. Walch and C. W. Bauschlicher, Jr., *Comparison of Ab Initio Quantum Chemistry with Experiment for Small Molecules* (Reidel, New York, 1985), pp. 17–51.
[4] A. L. Cabrera, J. F. Kirner, and J. N. Armor, J. Mater. Res. **6**, 71 (1990).
[5] S. Hymes, S. P. Muraka, C. Shepard, and W. A. Langford, J. Appl. Phys. **71**, 4623 (1992).
[6] M. Setton, J. Van der Spiegel, and B. Rothman, Appl. Phys. Lett. **57**, 357 (1990).
[7] R. Padiyath, J. Seth, S. V. Babu, and L. J. Matienzo, J. Appl. Phys. **73**, 2326 (1993).
[8] K. N. Tu, Appl. Phys. Lett. **27**, 221 (1975).
[9] A. Hiraki, Surf. Sci. **168**, 74 (1986).
[10] M. O. Aboelfotoh and L. Krusin-Elbaum, J. Appl. Phys. **70**, 3382 (1991).
[11] M. O. Aboelfotoh, A. Cros, B. G. Stevenson, and K. N. Tu, Phys. Rev. B **41**, 9819 (1990).
[12] See, e.g., M. D. Morse, J. B. Hopkins, P. R. R. Langridge-Smith, and R. E. Smalley, J. Chem. Phys. **79**, 5316 (1983).
[13] See, e.g., E. A. Rholfing, and J. J. Valentini, Chem. Phys. Lett. **126**, 113 (1986); R. H. Page and C. S. Gudemann, J. Chem. Phys. **94**, 39 (1991).
[14] See, e.g., C. R. Wang, S. Pollock, and M. M. Kappes, Chem. Phys. Lett. **166**, 26 (1990).
[15] A. O'Keefe, J. J. Scherer, A. L. Cooksy, R. Sheeks, J. Heath, and R. J. Saykally, Chem. Phys. Lett. **172**, 214 (1990).
[16] R. B. King, Z. Phys. D **18**, 189 (1991).
[17] I. Shim, J. E. Kingcade, Jr., and K. A. Gingerich, Z. Phys. D **7**, 261 (1987).
[18] I. Shim and K. A. Gingerich, Z. Phys. D **16**, 141 (1990).
[19] H. Haberlandt, Chem. Phys. **138**, 315 (1989).
[20] M. D. Morse, G. P. Hansen, P. R. R. Langridge-Smith, Lan-Sun Zheng, M. E. Geusic, D. L. Michalopoulos, and R. E. Smalley, J. Chem. Phys. **80**, 5400 (1984).
[21] E. M. Spain and M. D. Morse, J. Chem. Phys. **97**, 4605 (1992).
[22] G. A. Bishea, C. A. Arrington, J. M. Behm, and M. D. Morse, J. Chem. Phys. **95**, 8765 (1991).
[23] G. Herzberg, *Spectra of Diatomic Molecules* (Van Nostrand, New York, 1953), Chap. VI D.
[24] A. O'Keefe, and D. A. G. Deacon, Rev. Sci. Instrum. **59**, 2544 (1988); see also A. J. Ramponi, F. P. Milanovich, T. Kan, and D. Deacon, Appl. Opt. **27**, 4606 (1988); J. M. Herbelin, J. A. McKay, M. A. Kwok, R. H. Ueunten, D. S. Urevig, D. J. Spencer, and D. J. Benard, *ibid*. **19**, 144 (1980); J. M. Herbelin and J. A. McKay, *ibid*. **20**, 3341 (1980); D. Z. Anderson, J. C. Frisch, and C. S. Masser, *ibid*. **23**, 1238 (1984).
[25] D. Romanini and K. K. Lehmann, J. Chem. Phys. **99**, 6287 (1993).
[26] M. Lester *et al.* (private communication).

Downloaded¬19¬May¬2006¬to¬131.215.225.175. Redistribution¬subject¬to¬AIP¬license¬or¬copyright,¬see¬http://jcp.aip.org/jcp/copyright.jsp

[27] T. Yu and M. C. Lin, J. Am. Chem. Soc. **115**, 4371 (1993).
[28] G. Meijer, M. G. H. Boogaarts, R. T. Jongma, D. H. Parker, and A. M. Wodtke, Chem. Phys. Lett. **217**, 112 (1994).
[29] E. Hecht and A. Zajac, *Optics* (Addison–Wesley, Reading 1980), p. 2835.
[30] J. J. Scherer, J. B. Paul, A. O'Keefe, and R. J. Saykally, Chem. Rev. (submitted).
[31] D. E. Powers, S. G. Hansen, M. E. Geusic, D. L. Michalopoulos, and R. E. Smalley, J. Phys. Chem. **86**, 2556 (1982).
[32] Siegmann, *Lasers* (University Science Books, Mill Valley, 1986), Chap. 27.
[33] W. C. Wiley and I. H. Mclaren, Rev. Sci. Instrum. **26**, 1150 (1955).
[34] R. M. Jordan Co., Grass Valley, California.
[35] A. E. Douglas, Can. J. Phys. **35**, 71 (1957).
[36] R. D. Verma and P. A. Warsop, Can. J. Phys. **43**, 152 (1963).
[37] S. M. Beck, J. Chem. Phys. **87**, 4223 (1987).
[38] S. M. Beck, J. Chem. Phys. **90**, 6306 (1989).
[39] J. L. Dunham, Phys. Rev. **41**, 721 (1932).
[40] G. Herzberg, *Spectra of Diatomic Molecules* (Van Nostrand, New York, 1953), p. 248.
[41] A. Kratzer, Z. Phys. **3**, 289 (1920).
[42] G. Riekert, P. Lamparter, and S. Steeb, Z. Für Metall. **72**, 765 (1981).
[43] A. Van der Auwera-Mahieu, N. S. McIntyre, and J. Drowart, Chem. Phys. Lett. **4**, 198 (1969).
[44] R. F. Barrow, W. J. M. Gissane, and D. N. Travis, Nature **201**, 603 (1964); R. Houdart and J. Schamps, J. Phys. B **6**, 2478 (1973).
[45] K. A. Gingerich, J. Chem. Phys. **50**, 5426 (1969).

Downloaded¬19¬May¬2006¬to¬131.215.225.175. Redistribution¬subject¬to¬AIP¬license¬or¬copyright,¬see¬http://jcp.aip.org/jcp/copyright.jsp